ACS APPLIED MATERIALS & INTERFACES

Research Article

www.acsami.org

Microwave-Assisted Fabrication of Titanium Implants with Controlled Surface Topography for Rapid Bone Healing

Muralithran G. Kutty,[†,‡] Alok De,[§,∥] Sarit B. Bhaduri,[⊥] and Alireza Yaghoubi*[,#]

[†]Department of Restorative Dentistry, Faculty of Dentistry, University of Malaya, Kuala Lumpur 50603, Malaysia

[‡]Department of Materials and Metallurgical Engineering, University of Idaho, Moscow, Idaho 83844, United States

[§]Department of Veterinary and Comparative Anatomy, Washington State University, Pullman Washington 99164, United States

[∥]Deptartment of Obstetrics and Gynecology, School of Medicine, University of Missouri-Kansas City, Kansas City, Missouri 64108, United States

[⊥]Multi-Functional Materials Laboratory, University of Toledo, Toledo, Ohio 43606, United States

[#]Center for High Impact Research, University of Malaya, Kuala Lumpur 50603, Malaysia

Supporting Information

ABSTRACT: Morphological surface modifications have been reported to enhance the performance of biomedical implants. However, current methods of introducing graded porosity involves postprocessing techniques that lead to formation of microcracks, delamination, loss of fatigue strength, and, overall, poor mechanical properties. To address these issues, we developed a microwave sintering procedure whereby pure titanium powder can be readily densified into implants with graded porosity in a single step. Using this approach, surface topography of implants can be closely controlled to have a distinctive combination of surface area, pore size, and surface roughness. In this study, the effect of various surface topographies on *in vitro* response of neonatal rat calvarial osteoblast in terms of attachment and proliferation is studied. Certain graded surfaces nearly double the chance of cell viability in early stages (∼one month) and are therefore expected to improve the rate of healing. On the other hand, while the osteoblast morphology significantly differs in each sample at different periods, there is no straightforward correlation between early proliferation and quantitative surface parameters such as average roughness or surface area. This indicates that the nature of cell-surface interactions likely depends on other factors, including spatial parameters.

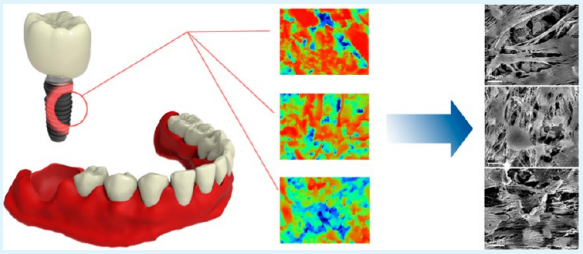

KEYWORDS: *bone tissue engineering, surface porosity, roughness, microwave sintering, cell proliferation, osteoblast*

1. INTRODUCTION

Titanium and titanium alloys, owing to their high strength, relatively low elastic modulus, and good anchorage to the living hard tissues,[1] have been for the past several decades among the most widely utilized materials for total joint replacements[2] as well as dental implants.[3,4]

Osteogenesis in the vicinity of metallic implants having a bioinert nature largely depends on the surface characteristics of the implants, which dictate the primary interactions with osteoblast cells via adsorption of proteins.[5] Surface modifications whether morphological[6,7] or chemical via introduction of biomolecules,[8] oxides,[9] and bioceramics[10,11] have been reported to positively influence cell viability and proliferation. Passive oxide layers, which are usually added to the implants using electrochemical methods,[12] are in particular desirable because, in addition to reinforcing ingrowth for a better biological fixation of the implants, they improve corrosion resistance and durability.[13] More recently, modified metallic substrates have even been used to accelerate the differentiation process. Orza et al. have shown that complex nanostructures composed of metalized collagens have the ability to sustain mesenchymal stem cell differentiation and may be potentially used for delivery of genes for *in vivo* transplantation.[14,15]

However, despite such advances, development of optimal implants with special emphasis on surface morphology and its influence on interfacial growth as well as shear-load bearing capacity is still being actively pursued.[4]

In general, surface topography, which may vary depending on the processing technique, is often quantified in terms of porosity, roughness, and surface area. Among these, porosity, whether closed or open, is of special importance since it provides a template for the extracellular matrices (ECMs) to adhere to and indirectly contributes to a larger surface area and relatively better bioactivity as a result.[16] Moreover, interconnected pores serve as a network of vascular canals ensuring the appropriate supply of blood and nutrition to the internally growing tissues. Because of their reduced Young's modulus[17] and decreased resistance to motion and wear loss,[18] porous

Received: May 14, 2014
Accepted: August 6, 2014
Published: August 6, 2014

   dx.doi.org/10.1021/am502967n | ACS Appl. Mater. Interfaces 2014, 6, 13587−13593

implants have also been reported to minimize resorption of adjacent osseous tissues and thereby have prolonged lifetime. Furthermore, in clinical trials, it has been demonstrated that implant surface roughness can increase the amount of translocated bone particles and thereby lead to beneficial osteogenic responses similar to how autografts improve peri-implant osteogenesis.[19]

To date, the most common technique used to fabricate porous titanium implants involves sintering of metal powder, beads, or fibers onto the surface of a dense solid, which, due to stress concentration, is often accompanied by microcracking, delamination, and loss of fatigue strength.[20,21] Other methods rely on electrodischarge compaction (EDC) of loosely packed atomized titanium powders[22] or plasma spraying to create a porous surface,[23,24] which, even though it results in advantageous morphological features, leads to poor mechanical properties associated with strained lamellar arrangements and degradation of microstructures at high temperatures.[21,25] Direct sintering of coarse-beaded titanium to achieve a functionally porous structure has also proven to possess unsatisfactory microstructure without secondary additives such as silicon, and even then local stress concentration may be problematic.[26]

More recent approaches similarly suffer from several drawbacks. For example, in sand-blasted implants, the embedded residues of blasting materials are not often completely removed even after ultrasonic or acid cleaning. These particles later may interfere with interactions between the implant and its surrounding tissues.[4] Chemical treatments by strong acids either via etching or anodizing on the other hand, beside the environmental concerns, may lead to hydrogen embrittlement of metallic implants.[27]

In recent years, our research interest has been to simplify manufacturing processes for the fabrication of metallic components including those with biomedical applications. From that viewpoint, we developed a one-step microwave processing technique to fabricate surfaces with graded porosity,[28] which are of great importance to osseointegration of implants.[16] As opposed to conventional manufacturing techniques, our one-step technique uses a powder metallurgy route that effectively eliminates the adverse effects of postprocessing (e.g., contamination, stress concentration, etc.), while simultaneously streamlining the process. The main aspect of this novel microwave sintering process is the peculiar way microwaves interact with materials in general and more importantly with metals in particular.[29] Just like any other microwave-active material, microwaves do get absorbed by metallic particulates, but due to a more pronounced absorption in the interiors, there is significant dissipation of heat from the surface, thus creating a thin layer of graded porosity. Our functionally graded implants sintered by microwave typically have a 100−200 μm thick porous surface with the size of the interconnected pores ranging from 10 to 100 μm depending on the initial powder.

In this study, we evaluate the response of neonatal rat osteoblast in terms of attachment and proliferation rate for different surface topographies of microwave-sintered implants. The positive effect of graded porosity on the early improvement of cell viability is remarkable; however, a long-term correlation between specific surface parameters such as roughness or surface area and an enhanced biological response cannot be deduced. It is likely that those spatial features such as frequency of peaks or valleys, which cannot be readily quantified, play a significant role in cell-surface interactions.

2. EXPERIMENTAL DETAILS

2.1. Microwave Sintering. Titanium disks with surface pores were prepared by sintering 99.9% pure titanium powder (Alfa Aesar, Ward Hill, MA) of different particle sizes (45, 75, and 150 μm). The powders were uniaxially pressed under 40 MPa into discs of 30 mm in diameter and 4 mm in thickness. An industrial microwave furnace (Microwave Materials Technology, Knoxville, TN) with a variable-power output magnetron source capable of operating up to 3 kW at 2.45 GHz was used for processing. The experimental setup consisted of a microwave generator coupled to a cavity where samples were placed in a flask made of Pyrex glass and dense SiC strips as susceptors. The flask was first evacuated and backfilled with argon, and finally the whole unit was placed within a box made of Al_2O_3 fiberboard. The low-density fibers were insulating but not significantly absorptive at the operating frequency. Further details of the processing technique employed to produce the samples have been reported elsewhere.[28]

The sintered disks were then ultrasonically cleaned thoroughly in absolute acetone for 10 min and dried in oven at 40 °C. The samples were subsequently sterilized by autoclaving at 130 °C for 20 min before cell culture.

2.2. Optical Profilometry. The surface topography of samples was analyzed by a noncontact optical profilometer (NT-2000, WYKO Corp.) with a vertical scanning range from 1 nm to 500 μm. A total of five scans were carried out on each sample using the Vertical Scanning Interferometry (VSI) mode. Three-dimensional topographies were reconstructed with a magnification of 25× giving a surface scan area of 0.035 mm^2. Statistical analysis of the data yielded surface properties R_a, R_q, R_z, and R_t. Surface area of the samples, that is, the fully exposed three-dimensional surface area being analyzed, including peaks and valleys, was also calculated and compared against the lateral surface area of 0.035 mm^2 (refer to Section S1 of the Supporting Information for the detailed procedure).

2.3. Laser Scanning Confocal Microscopy. A Bio-Rad MRC 1000 laser scanning confocal microscope (LSCM) operating with an argon-ion source (wavelength, 488 nm) was used to study the variations of morphology with depth. The scan area was a 512 × 512 pixel array corresponding to 1 mm^2.

2.4. Cell Culture. *In vitro* studies on microwave-sintered titanium samples were conducted using a culture of neonatal rat calvarial osteoblast.[30] The osteoblast cells were isolated from 18 to 21 day Sprague−Dawley rat fetuses and placed in ice cold Hank's Balanced Salt Solution (HBSS) containing 1% Fungai-Bact, 0.1% bovine serum albumin, and 200 mM ascorbic acid. Use of animal tissues followed an approved animal use protocol and satisfied the requirement of the Animal Ethics Committee. The cells were washed three to four times in HBSS, another time in Dulbecco's modified Eagle medium (DMEM) and then incubated with 1 mg/mL trypsin (made in DMEM) for 1 h at 37 °C. The large pieces of skull were removed and then centrifuged at 900 rpm for 5 min. The pellet was collected and resuspended in 5 mL of DMEM. The cells were grown in DMEM (Sigma) containing 10% fetal bovine serum (Hyclone Laboratories) and subsequently plated in 24 well plates on borosilicate glass (as control) and on titanium samples at 37 °C for 1, 2, 4, and 8 weeks. Each well had ∼20 000 cells in the media, which were applied with great care onto the upper porous surface of each disk to avoid any unwanted spillage or attachment of the cells to the surrounding plastic surface of the well. The plates were then placed in a tissue culture incubator (37 °C, 5% CO_2). The culture media, DMEM with 5% fetal bovine serum (Hyclone Laboratories), was changed every 3 d.

2.5. Statistical Significance. Cell viability was measured at different periods (1, 2, 4, and 8 weeks) by counting the number of trypsinized cells using Trypan blue exclusion method. After this period, the samples were freeze-dried for observation under the scanning electron microscope (SEM). In total, 144 pieces were prepared; 12 for each three particle size and each four periods of cell culture. All graphical data are represented as mean + S.D.M. Significance was tested using one way repeated measures ANOVA. $p < 0.05$ was considered significant.

Table 1. Roughness, Surface Area, and Pore Size Data of the Sintered Samples of Different Particle Sizes ± Standard Deviation for N =5

particle size (μm)	R_a (μm)	R_q (μm)	R_z (μm)	R_t (μm)	surface area (mm^2)	pore size (μm)
45	6.39 ± 1.01	8.06 ± 1.00	42.84 ± 3.30	45.37 ± 3.35	0.074 ± 0.003	60−100
75	5.37 ± 0.16	6.86 ± 0.22	44.44 ± 1.00	46.71 ± 1.79	0.082 ± 0.001	30−80
150	5.07 ± 0.06	6.47 ± 0.16	43.40 ± 5.55	46.87 ± 7.02	0.072 ± 0.002	10−60

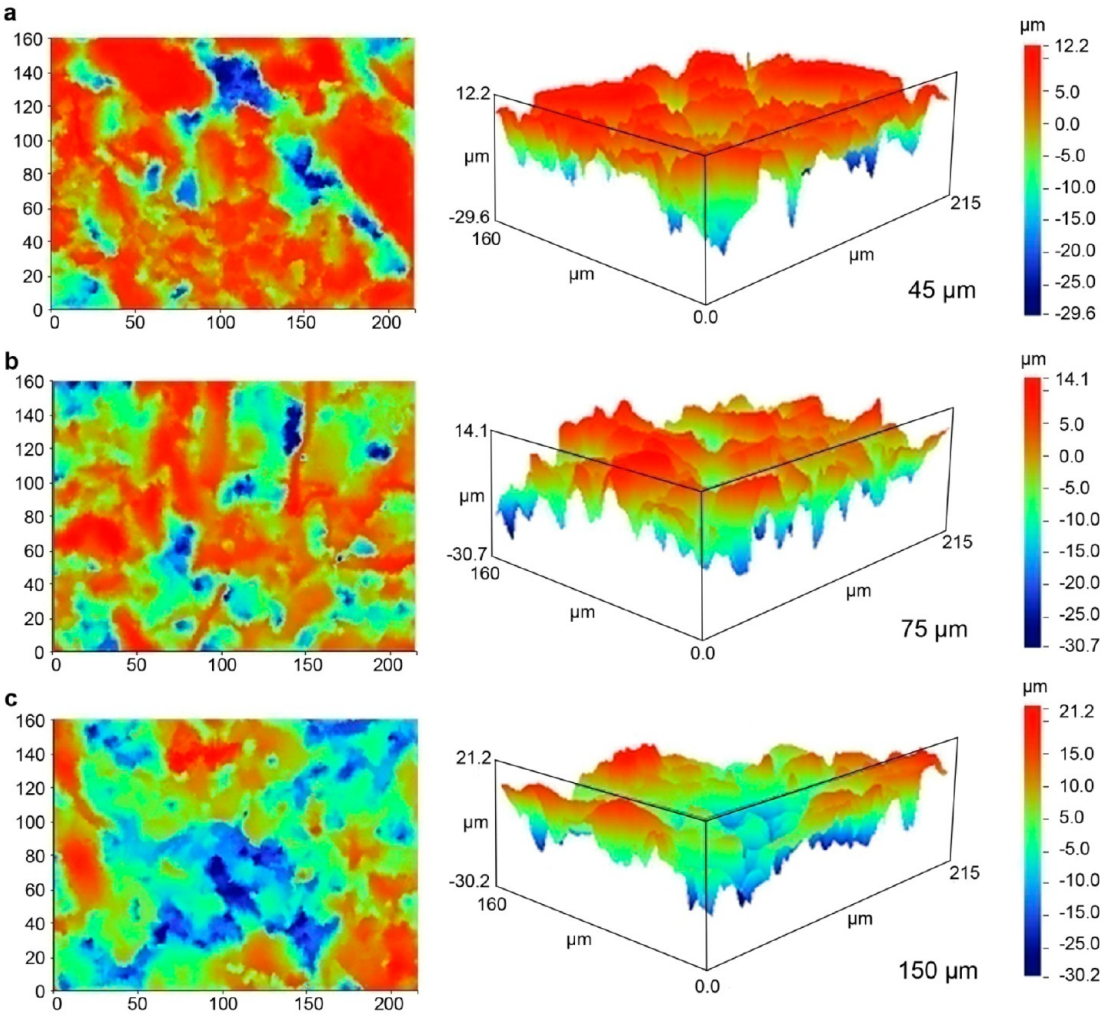

Figure 1. Surface topography of titanium samples of different particle sizes. (a) 45 μm, (b) 75 μm, and (c) 150 μm. The two-dimensional maps and the three-dimensional scanning surface reconstructions complement the micrographs of Figure 3 by clearly denoting the highest peaks (red) as well as the lowest valleys (blue).

3. RESULTS AND DISCUSSION

3.1. Surface Topography and Composition. The surface of a typical microwave-sintered sample shows intricate patterns of interconnected pores as opposed to the polished titanium, which exhibit fine grooves, a few microns in depth (see Supporting Information, Figure S2 for supplementary SEM micrographs). As presented in Table 1, the size of pores generally decreases with increasing particle size of the initial titanium powder. Similarly, with an increase in particle size, there is a decreasing trend for the average surface roughness R_a. The disks sintered from 45 μm powder had a surface roughness of 6.39 ± 1.01 μm as compared to 5.07 ± 0.06 μm for those prepared using the 150 μm powder.

Variations in surface area with different particle sizes, calculated from topography analyses, showed that the 45 and 150 μm samples had virtually identical surface areas of 0.074 ± 0.003 mm^2 and 0.072 ± 0.002 mm^2, respectively. The 75 μm samples on the other hand exhibited a larger surface area of 0.082 ± 0.001 mm^2, a nearly 14% increase.

The two-dimensional surface topographic maps as well as the three-dimensional reconstructions (Figure 1) clearly demonstrate the significant variation in surface roughness and morphology for each sample. Here, reduction in surface roughness with increasing particle size is evident from the fact that the darker (red) regions, which correspond to the high peaks of the rough surface are most common in 45 μm samples. On the other hand, the implant prepared from 150 μm powder has more deep valleys (blue), and the sample made from 75 μm powder is placed somewhere in between, having a relatively even combination of peaks and valleys. This spatial variation is comparatively more challenging to study in terms of the common average roughness R_a. Therefore, in this specific case

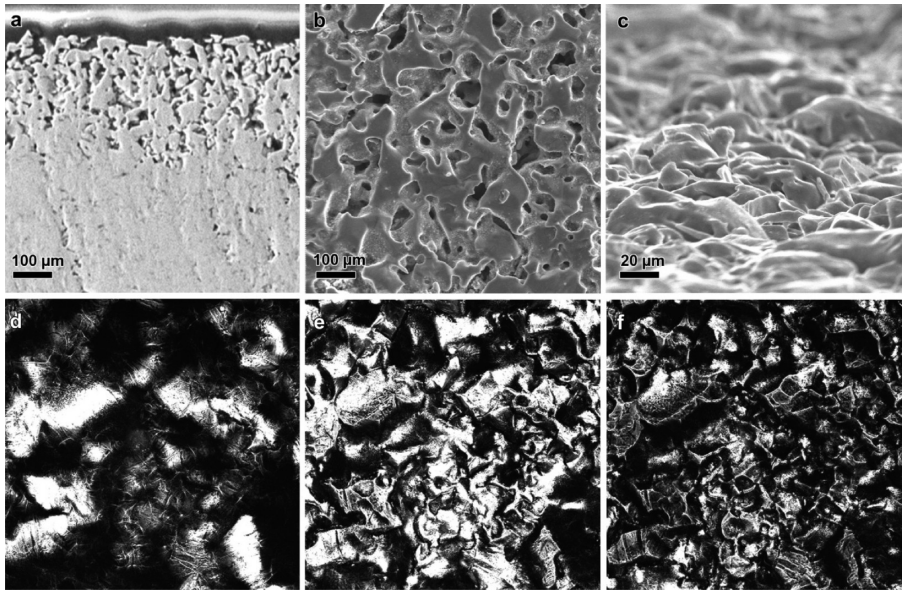

Figure 2. Interconnected pores are depicted in SEM micrograph taken from the cross-section (a), top (b), and side (c). Corresponding LSCM images showing the top surface (d) and variations in topography at a depth of 20 μm (e) and 40 μm (f). The scan area was a 512 × 512 pixel array corresponding to 1 mm^2. A set of more detailed images captured at smaller depth profiles (2 and 5 μm) can be viewed in Supporting Information, Figure S3.

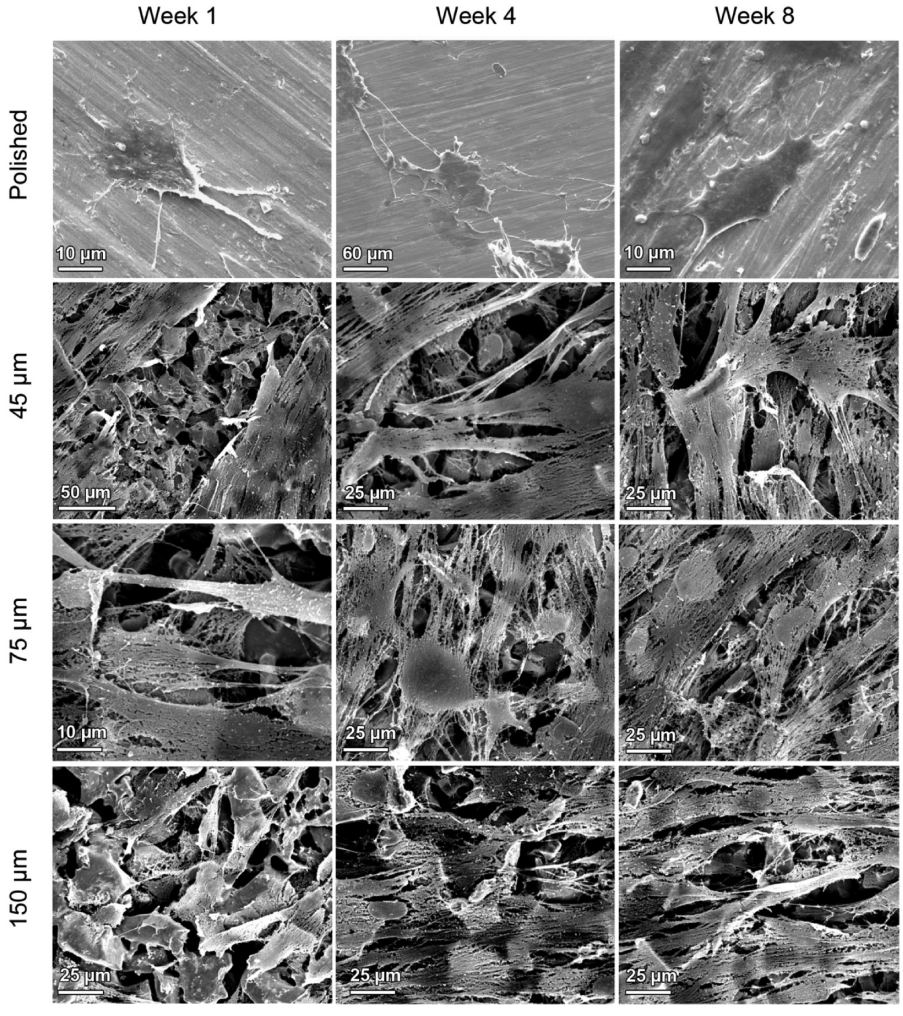

Figure 3. SEM micrographs of osteoblast cells grown within different durations on functionally porous samples prepared from 45, 75, and 150 μm particle sizes.

and for many other functionally porous implants, we believe that the surface topography is best represented in terms of R_z, the average maximum height of the profile, which is the average of the greatest peak-to-valley separations and is calculated as $R_z = N^{1-}[(H_1 + H_2 + \cdots H_N) - (L_1 + L_2 + \cdots L_N)]$, where H_i denotes the highest points and L_i denotes the lowest points found in the evaluation area (see Supporting Information, Section S1 for more details). While the R_z roughness is a good relative standard for comparing the samples fabricated from different powders, in comparing the optimal surface roughness and area with other studies, another set of problems arises. The method described here based on microwave sintering is a bottom-up approach as dielectric heating begins at the core and heat is dissipated from the surface. Unlike other top-down surface modification techniques such as sand blasting or acid etching, the porous structure on the surface can be morphologically more complex with interconnected pores in deeper region not being accounted for properly in profilometry. This topographic complexity is clearly shown in cross-sectional SEM micrographs of Figure 2 as well as the corresponding LSCM images. The challenges of defining a precise optimum range for roughened implants have been also discussed extensively by Wenneberg and Albrektsson.[31] By analyzing various studies, it was found that either the samples were prepared using different methods and therefore could not have been directly compared or, upon using similar approaches, lack of a standardized technique for quantifying surface parameters made a broadly applicable conclusion infeasible.

With regard to surface composition, surface pores formed using this method similar to those prepared through electrochemical[12] or chemical routes[32] are covered with a thin layer of oxide as indicated by X-ray photoelectron spectroscopy (XPS), although in our method, this is likely to originate from passive oxidation by atmospheric residue in the sintering environment (see Supporting Information, Figure S4). The generally positive *in vitro* results obtained for titanium implants are normally attributed to the presence of this passive layer, which, even though it may not chemically bond to the bone tissues,[33] contributes to adhesion of leukocytes and subsequently to their interaction with proteins by enhancing the surface energy.[34]

In terms of crystallinity, no secondary phase was detected in the X-ray diffraction profile (see Supporting Information, Figure S5), and all the observed peaks were related to pure α-Ti.

3.2. Osteoblast Attachment and Morphology. SEM micrographs of Figure 3 show the increasing attachment of osteoblast cells cultured in 1, 4, and 8 weeks on different surface topographies. It is evident that there is a significant difference in cellular attachment and expansion on the smooth titanium surface as compared to the porous samples. In particular, partial attachment of cells on the polished surfaces appears to be significant; however, only on porous samples, the osteoblasts rapidly spread on the ECMs. Among a variety of samples with graded pores used for cell culture, in short-term (one week), those microwave-sintered from 75 μm powder induced the highest number of viable cells ($p \leq 0.01$ as compared to the control, see Figure 4) and also the largest extension of ECMs, while retaining the semispherical and protruded morphology of osteoblast cells. After two weeks, the number of cells was increased in all groups, although we did not see any significant variance.

Upon prolonging the culture to four weeks, the smooth titanium samples started to show considerably smaller traces of

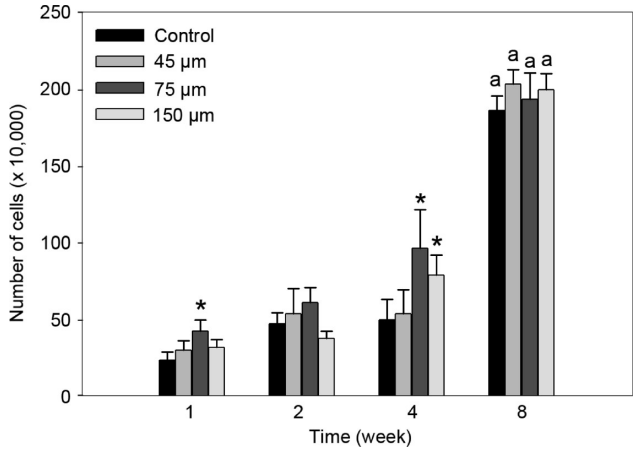

Figure 4. Osteoblasts were cultured in DMEM with 5% fetal bovine serum for 1, 2, 4, and 8 weeks on plastic or titanium substratum (fabricated from 45, 75, and 150 μm powder) as described under Methods. The values are means + S.D.M. of eight independent experiments. ∗ indicates $p < 0.05$ as compared with control group, and a indicates $p < 0.05$ as compared with weeks 1, 2, and 4.

collagen matrices interlinking the individual cells to one another. These cells appear to closely conform to the surface contours considering that unlike porous samples, their morphology is stretched toward regions where grooves are more pronounced. Within the same period (four weeks), the 45 and 150 μm samples ($p = 0.014$), even though at a slower rate in comparison to the 75 μm samples ($p \leq 0.001$), showed a significant improvement in cellular attachment. After eight weeks, the number of cells was significantly more in all groups including the control substratum in comparison to earlier time points ($p \leq 0.001$), but the cells were morphologically different. The polished surfaces supported further cell growth only to give rise to what appeared to be a conditioning sublayer of flattened cells for further growth of ECMs on the top surface (similar to bottom layers in porous samples). On the contrary, all the porous samples exhibited very dense cell population regardless of surface parameters to the extent that their underlying metal surface was barely visible. Overall, it is evident that cell cycle takes different turns depending on the surface topography regardless of cell viability in each stage (Figure 4). It must be emphasized, however, that topographical features and their effects toward biological pathways often cannot be easily quantified.[35] Therefore, even though in some cases it is possible to use numerical data such as surface area or roughness to describe surface-cell interactions, such implications are only true for certain stages of growth. For instance, comparing the cell viability for the 45 and 150 μm samples with nearly identical surface areas, we observe that by week two, the former had a considerably larger number of viable cells, which remained constant until week four. Interestingly, the number of cells on the 150 μm sample by this stage rapidly grew to surpass the 45 μm sample by almost 50%. One may argue that the higher average surface roughness R_a of the 45 μm sample could have promoted cell attachment in short-term; however, looking at the 75 μm sample, which had a lower surface roughness R_a but a higher surface area and a remarkably better cell viability in every stage from week one to week four, a more complex underlying mechanism is inferred.

As discussed in section 3.1, surface topography of functionally graded samples with textures on limited-access surfaces

such as grooves and pores, particularly where the typical presence of high peaks or deep valleys is of functional significance, is best represented by R_z roughness. Here we can simplify the topography-cell response correlation by taking the R_z roughness to be the most effective indicator of cell attachment. The rate of early cell viability in samples fabricated from 75, 150, and 45 μm powder can be associated with a higher R_z value of 44.44 ± 1.00, 43.40 ± 5.55, and 42.84 ± 3.30 μm, respectively, but as a matter of fact, these numbers only represent the average value, and their variance is not significant enough (as compared to their standard deviation) to warrant any actual causation. Furthermore, it was noted earlier that the two porous samples prepared from 45 and 150 μm particles had approximately similar surface areas, but from week two to week four, their rate of attachment suddenly reversed, disproving the idea that a higher rate of proliferation is due to a larger surface area. This series of observations, as long as the biological aspects are concerned, is consistent with the dynamic nature of the cell-cycle progression in osseous tissues. The regulatory signals corresponding to each phenotypic expression and subsequently to the time-dependent behavior of cells often function in a localized manner,[36] whereas most numerical trends in topographical changes such as average surface roughness or surface area are only statistically significant for a large scan area. An example in favor of this argument is the distinct cellular morphology on 45 and 75 μm samples signified by the more rounded and protruded shape of the osteoblasts in the latter. In this regard, it has to be considered that on a submicron scale, the concentrated presence of vinculin adhesion plaques in the proximity of lacunae is the main reason behind a more rounded shape.[37]

The underlying mechanism behind variations in phenotypic expression at the interface of bone and implant is not the scope of this report and will be addressed elsewhere based on the relevant proteins and genes assays, but these findings are essentially in agreement with earlier reports[38] that have indicated a similar change of behavior, suggesting that the adhesion rate for rougher surfaces was slower, while cells appeared to have advanced more through their cycle in comparison to smooth surfaces.

Additionally, pores may significantly influence vascularization and ingrowth (see the SEM micrographs of Supporting Information, Figure S6, for example). Müller and colleagues have also reported that human osteoblasts, especially under perfusion, are able to grow into pores, form specific phenotypes, and express bone matrix proteins.[39] However, there is no general consensus about the optimal range of pore size.[40] St. Pierre et al. have reported that variations in pore size showed noticeable effects only during proliferation.[41] Despite earlier studies recommending a 100 μm limit, Itälä et al. also showed that there is no pore size requisite for bone ingrowth, and under nonload-bearing conditions, secondary osteonal structures pore sizes range from 50 to 125 μm.[42]

4. CONCLUSIONS

In summary, we established a facile technique for fabrication of implants with biologically desirable surface topography by microwave sintering of titanium powder. As compared to other methods, which involve postprocessing, this single-step process is expected to improve durability as well as mechanical properties of implants. We further demonstrated that surface topography varies distinctively as a function of the initial particle size and subsequently influence the surface-cell interaction. Implants with graded porosity promoted a better rate of cell viability in early stages of culture. This approach enables the time- and cost-effective fabrication of personalized implants based on the particular conditions of a patient. While for any practical case, it is safe to assume that microwave-sintered implants with graded porosity accelerate bone healing, the detailed mechanism cannot be simply explained in terms of strict numerical measurements such as surface roughness and area. Further work, especially with regard to gene expressions and phenotypic markers, is required to reveal the influence of interfacial phenomena on cell growth cycle. *In vivo* tests of implants prepared using this technique are in progress and will be reported shortly along with more detailed assays.

■ ASSOCIATED CONTENT

Supporting Information

Detailed procedure for calculating the surface parameters, supplementary LSCM images, electron micrographs, XPS and XRD profiles. This material is available free of charge via the Internet at http://pubs.acs.org.

■ AUTHOR INFORMATION

Corresponding Author

*E-mail: yaghoubi@siswa.um.edu.my. Phone: +60173470750. Fax: +60379677727.

Notes

The authors declare no competing financial interest.

■ ACKNOWLEDGMENTS

This study was funded by NSF under Grant No. DMI-0085100. We thank Martine LeBerge at Clemson Univ. for providing access to the profilometer. A.Y. acknowledges financial support from Univ. of Malaya under UM.C/625/1/HIR/MOHE/CHAN/09.

■ REFERENCES

(1) Deguchi, T.; Takano-Yamamoto, T.; Kanomi, R.; Hartsfield, J. K.; Roberts, W. E.; Garetto, L. P. The Use of Small Titanium Screws for Orthodontic Anchorage. *J. Dent. Res.* **2003**, *82*, 377−381.

(2) Long, M.; Rack, H. J. Titanium Alloys in Total Joint Replacement—A Materials Science Perspective. *Biomaterials* **1998**, *19*, 1621−1639.

(3) Verket, A.; Lyngstadaas, S. P.; Rønold, H. J.; Wohlfahrt, J. C. Osseointegration of Dental Implants in Extraction Sockets Preserved with Porous Titanium Granules—An Experimental Study. *Clin. Oral Implants Res.* **2014**, *25*, e100−e108.

(4) Le Guéhennec, L.; Soueidan, A.; Layrolle, P.; Amouriq, Y. Surface Treatments of Titanium Dental Implants for Rapid Osseointegration. *Dent. Mater.* **2007**, *23*, 844−854.

(5) Yazici, H.; Fong, H.; Wilson, B.; Oren, E. E.; Amos, F. A.; Zhang, H.; Evan, J. S.; Snead, M. L.; Sarikaya, M.; Tamerler, C. Biological Response on a Titanium Implant-Grade Surface Functionalized with Modular Peptides. *Acta Biomater.* **2013**, *9*, 5341−5352.

(6) Martin, J. Y.; Schwartz, Z.; Hummert, T. W.; Schraub, D. M.; Simpson, J.; Lankford, J., Jr.; Dean, D. D.; Cochran, D. L.; Boyan, B. D. Effect of Titanium Surface Roughness on Proliferation, Differentiation, and Protein Synthesis of Human Osteoblast-Like Cells (MG63). *J. Biomed. Mater. Res.* **1995**, *29*, 389−401.

(7) Deligianni, D. D.; Katsala, N.; Ladas, S.; Sotiropoulou, D.; Amedee, J.; Missirlis, Y. F. Effect of Surface Roughness of the Titanium Alloy Ti−6Al−4V on Human Bone Marrow Cell Response and on Protein Adsorption. *Biomaterials* **2001**, *22*, 1241−1251.

(8) Cai, K.; Rechtenbach, A.; Hao, J.; Bossert, J.; Jandt, K. D. Polysaccharide-Protein Surface Modification of Titanium via a Layer-

by-Layer Technique: Characterization and Cell Behaviour Aspects. *Biomaterials* **2005**, *26*, 5960−5971.
(9) Pan, J.; Liao, H.; Leygraf, C.; Thierry, D.; Li, J. Variation of Oxide Films on Titanium Induced by Osteoblast-like Cell Culture and the Influence of an H_2O_2 Pretreatment. *J. Biomed. Mater. Res.* **1998**, *40*, 244−256.
(10) Ripamonti, U.; Roden, L. C.; Renton, L. F. Osteoinductive Hydroxyapatite-Coated Titanium Implants. *Biomaterials* **2012**, *33*, 3813−3823.
(11) Afshar-Mohajer, M.; Yaghoubi, A.; Ramesh, S.; Bushroa, A. R.; Chin, K. M. C.; Tin, C. C.; Chiu, W. S. Electrophoretic Deposition of Magnesium Silicates on Titanium Implants: Ion Migration and Silicide Interfaces. *Appl. Surf. Sci.* **2014**, DOI: 10.1016/j.apsusc.2014.04.033.
(12) Sul, Y. T.; Johansson, C. B.; Petronis, S.; Krozer, A.; Jeong, Y.; Wennerberg, A.; Albrektsson, T. Characteristics of the Surface Oxides on Turned and Electrochemically Oxidized Pure Titanium Implants up to Dielectric Breakdown: the Oxide Thickness, Micropore Configurations, Surface Roughness, Crystal Structure and Chemical Composition. *Biomaterials* **2002**, *23*, 491−501.
(13) Schüpbach, P.; Glauser, R.; Rocci, A.; Martignoni, M.; Sennerby, L.; Lundgren, A. K.; Gottlow, J. The Human Bone−Oxidized Titanium Implant Interface: A Light Microscopic, Scanning Electron Microscopic, Back-Scatter Scanning Electron Microscopic, and Energy-Dispersive X-Ray Study of Clinically Retrieved Dental Implants. *Clin. Implant Dent. Relat. Res.* **2005**, *7*, s36−s43.
(14) Orza, A.; Soritau, O.; Olenic, L.; Diudea, M.; Florea, A.; Rus Ciuca, D.; Mihu, C.; Casciano, D.; Biris, A. S. Electrically Conductive Gold-coated Collagen Nanofibers for Placental-Derived Mesenchymal Stem Cells Enhanced Differentiation and Proliferation. *ACS Nano* **2011**, *5*, 4490−4503.
(15) Orza, A. I.; Mihu, C.; Soritau, O.; Diudea, M.; Florea, A.; Matei, H.; Balici, S.; Mudalige, T.; Kanarpardy, G. K.; Biris, A. S. Multistructural Biomimetic Substrates for Controlled Cellular Differentiation. *Nanotechnology* **2014**, *25*, 065102−065115.
(16) Simmons, C. A.; Valiquette, N.; Pilliar, R. M. Osseointegration of Sintered Porous-Surfaced and Plasma Spray-coated Implants: An Animal Model Study of Early Postimplantation Healing Response and Mechanical Stability. *J. Biomed. Mater. Res.* **1999**, *47*, 127−138.
(17) Zhu, K.; Li, C.; Zhu, Z.; Liu, C. S. Measurement of the Dynamic Young's Modulus of Porous Titanium and Ti6Al4V. *J. Mater. Sci.* **2007**, *42*, 7348−7353.
(18) Grądzka-Dahlke, M.; Dąbrowski, J. R.; Dąbrowski, B. Characteristic of the Porous 316 Stainless Steel for the Friction Element of Prosthetic Joint. *Wear* **2007**, *263*, 1023−1029.
(19) Tabassum, A.; Walboomers, F.; Wolke, J. G.; Meijer, G. J.; Jansen, J. A. The Influence of Surface Roughness on the Displacement of Osteogenic Bone Particles during Placement of Titanium Screw-Type Implants. *Clin. Implant Dent. Relat. Res.* **2011**, *13*, 269−278.
(20) Wolfarth, D.; Ducheyne, P. Effect of a Change in Interfacial Geometry on the Fatigue Strength of Porous-coated Ti−6Al−4V. *J. Biomed. Mater. Res.* **1994**, *28*, 417−425.
(21) Kohn, D. H.; Ducheyne, P. A Parametric Study of the Factors Affecting the Fatigue Strength of Porous Coated Ti−6Al−4V Implant Alloy. *J. Biomed. Mater. Res.* **1990**, *24*, 1483−1501.
(22) Qiu, J.; Dominici, J. T.; Lifland, M. I.; Okazaki, K. Composite Titanium Dental Implant Fabricated by Electro-Discharge Compaction. *Biomaterials* **1997**, *18*, 153−160.
(23) Yang, Y. Z.; Tian, J. M.; Tian, J. T.; Chen, Z. Q.; Deng, X. J.; Zhang, D. H. Preparation of Graded Porous Titanium Coatings on Titanium Implant Materials by Plasma Spraying. *J. Biomed. Mater. Res.* **2000**, *52*, 333−337.
(24) De Santis, D.; Guerriero, C.; Nocini, P. F.; Ungersbock, A.; Richards, P.; Gotte, P.; Armato, U. Adult Human Bone Cells from Jaw Bones Cultured on Plasma-sprayed or Polished Surfaces of Titanium or Hydroxylapatite Discs. *J. Mater. Sci.: Mater. Med.* **1996**, *7*, 21−28.
(25) Chang, C. K.; Wu, J. S.; Mao, D. L.; Ding, C. X. Mechanical and Histological Evaluations of Hydroxyapatite-Coated and Noncoated Ti6Al4V Implants in Tibia Bone. *J. Biomed. Mater. Res.* **2001**, *56*, 17−23.
(26) Thieme, M.; Wieters, K. P.; Bergner, F.; Scharnweber, D.; Worch, H.; Ndop, J.; Kim, T. J.; Grill, W. Titanium Powder Sintering for Preparation of a Porous Functionally Graded Material Destined for Orthopaedic Implants. *J. Mater. Sci.: Mater. Med.* **2001**, *12*, 225−231.
(27) Yokoyama, K.; Ichikawa, T.; Murakami, H.; Miyamoto, Y.; Asaoka, K. Fracture Mechanisms of Retrieved Titanium Screw Thread in Dental Implants. *Biomaterials* **2002**, *23*, 2459−2465.
(28) Kutty, M. G.; Bhaduri, S. B. Gradient Surface Porosity in Titanium Dental Implants: Relation Between Processing Parameters and Microstructure. *J. Mater. Sci.: Mater. Med.* **2004**, *15*, 145−150.
(29) Roy, R.; Agrawal, D.; Cheng, J.; Gedevanishvili, S. Full Sintering of Powdered-Metal Bodies in a Microwave Field. *Nature* **1999**, *399*, 668−670.
(30) Puleo, D. A.; Holleran, L. A.; Doremus, R. H.; Bizios, R. Osteoblast Responses to Orthopedic Implant Materials in Vitro. *J. Biomed. Mater. Res.* **1991**, *25*, 711−723.
(31) Wennerberg, A.; Albrektsson, T. Effects of Titanium Surface Topography on Bone Integration: A Systematic Review. *Clin. Oral Implants Res.* **2009**, *20* (s4), 172−184.
(32) Eriksson, C.; Lausmaa, J.; Nygren, H. Interactions Between Human Whole Blood and Modified TiO_2-Surfaces: Influence of Surface Topography and Oxide Thickness on Leukocyte Adhesion and Activation. *Biomaterials* **2001**, *22*, 1987−1996.
(33) Sul, Y. T. The Significance of the Surface Properties of Oxidized Titanium to the Bone Response: Special Emphasis on Potential Biochemical Bonding of Oxidized Titanium Implant. *Biomaterials* **2003**, *24*, 3893−3907.
(34) Anselme, K. Osteoblast Adhesion on Biomaterials. *Biomaterials* **2000**, *21*, 667−681.
(35) Lian, J. B.; Stein, G. S. Development of the Osteoblast Phenotype: Molecular Mechanisms Mediating Osteoblast Growth and Differentiation. *Iowa Orthop. J.* **1995**, *15*, 118−140.
(36) Mendonça, G.; Mendonça, D.; Simões, L. G.; Araújo, A. L.; Leite, E. R.; Duarte, W. R.; Aragão, F. J. L.; Cooper, L. F. The Effects of Implant Surface Nanoscale Features on Osteoblast-Specific Gene Expression. *Biomaterials* **2009**, *30*, 4053−4062.
(37) Hunter, A.; Archer, C. W.; Walker, P. S.; Blunn, G. W. Attachment and Proliferation of Osteoblasts and Fibroblasts on Biomaterials for Orthopaedic Use. *Biomaterials* **1995**, *16*, 287−295.
(38) Kieswetter, K.; Schwartz, Z.; Hummert, T. W.; Cochran, D. L.; Simpson, J.; Dean, D. D.; Boyan, B. D. Surface Roughness Modulates the Local Production of Growth Factors and Cytokines by Osteoblast-Like MG-63 Cells. *J. Biomed. Mater. Res.* **1996**, *32*, 55−63.
(39) Müller, U.; Imwinkelried, T.; Horst, M.; Sievers, M.; Graf-Hausner, U. Do Human Osteoblasts Grow Into Open-Porous Titanium? *Eur. Cell Mater.* **2006**, *11*, 8−15.
(40) Karageorgiou, V.; Kaplan, D. Porosity of 3D Biomaterial Scaffolds and Osteogenesis. *Biomaterials* **2005**, *26*, 5474−5491.
(41) St-Pierre, J. P.; Gauthier, M.; Lefebvre, L. P.; Tabrizian, M. Three-dimensional Growth of Differentiating MC3T3-E1 Pre-Osteoblasts on Porous Titanium Scaffolds. *Biomaterials* **2005**, *26*, 7319−7328.
(42) Itälä, A. I.; Ylänen, H. O.; Ekholm, C.; Karlsson, K. H.; Aro, H. T. Pore Diameter of More than 100 μm Is Not Requisite for Bone Ingrowth in Rabbits. *J. Biomed. Mater. Res.* **2001**, *58*, 679−683.